ACS APPLIED MATERIALS & INTERFACES

Research Article

www.acsami.org

Silver Nanoparticle-Embedded Microbubble as a Dual-Mode Ultrasound and Optical Imaging Probe

Fang Yang,*[,†] Qing Wang,[†] Zhuxiao Gu,[‡] Kun Fang,[†] Gerard Marriott,[§] and Ning Gu*[,†]

[†]State Key Laboratory of Bioelectronics, Jiangsu Key Laboratory for Biomaterials and Devices, School of Biological Science and Medical Engineering, Southeast University, Nanjing 210096, P. R. China

[‡]Key Laboratory of Developmental Genes and Human Diseases, Ministry of Education, Medical School, Southeast University, Nanjing 210009, P. R. China

[§]Department of Bioengineering, University of California, Berkeley, California 94720, United States

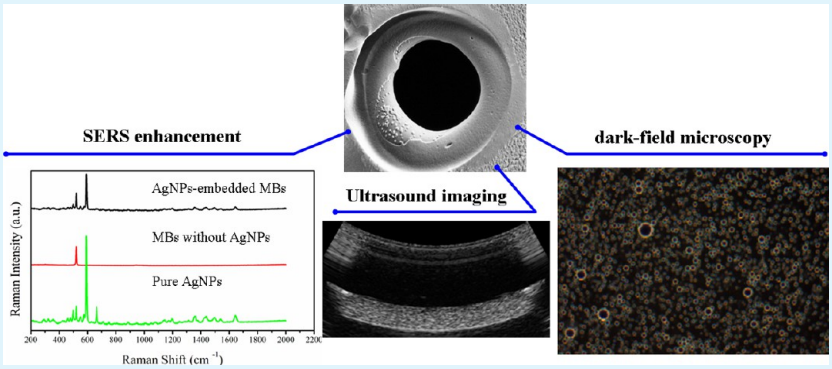

ABSTRACT: Microbubbles (MBs) coupled with nanoparticles represent a new class of multifunctional probe for multiscale biomedical imaging and drug delivery. In this study, we describe the development of multifunctional, microscale microbubble probes that are composed of a nitrogen gas core and a biocompatible polymer shell harboring silver nanoparticles (AgNPs). Ultrasound imaging studies show that the presence of AgNPs in the MB significantly improves the contrast of ultrasound images. The AgNPs within individual MB can be also imaged by using dark-field microscopy (DFM), which suggests that AgNPs in the polymer shell adopt multiple structural forms. AgNPs are released from the polymer shell following a brief exposure to an ultrasonic field and are subsequently taken up by living cells. AgNPs within labeled cells are imaged by DFM, while surface-enhanced Raman scattering is used to identify specific cytoplasmic biomolecules that bind to the surface of the AgNP. Collectively, these studies demonstrate the application of multifunctional MBs for micrometer scale contrast-enhanced ultrasound imaging, as vehicles for the ultrasound-based delivery of optical probes and drugs to cells, and for imaging of chemical sensing of individual nanopartiles within cells and tissue.

KEYWORDS: *microstructure surface, nanoparticles, diagnostics, ultrasound imaging, optical imaging*

1. INTRODUCTION

Molecular imaging in living organisms is realized by using a variety of imaging modalities that include computed tomography (CT), ultrasound, magnetic resonance imaging (MRI), optical imaging [bioluminescence, near-infrared (NIR) fluorescence, and surface-enhanced Raman scattering (SERS)], single-photon emission-computed tomography (SPECT), and positron emission tomography (PET). Ultrasound imaging is one of the most widely used for diagnostic imaging as it is noninvasive and easy to use, has a relatively low cost, and provides for real-time and deep imaging of vital organs.[1] However, ultrasound techniques can produce only low-resolution images of larger structures in a sample, and consequently, higher-resolution analysis of the samples requires the use of an ultrasound contrast-enhancing agent[2]or combining some other higher-resolution imaging modalities.[3,4]

Optical techniques such as bioluminescence, NIR fluorophores, and SERS from structured nanoparticles are capable of generating high-resolution images of a sample, i.e., with submicrometer resolution. Moreover, optical imaging is sensitive and allows the user to detect individual molecules or nanoparticles and to generate spatiotemporally resolved information about the optical probe within a living cells.[5] Several types of functionalized probes that integrate nanoparticles or nanomaterials have been used for *in vivo* optical imaging, including QDots (2−10 nm)[6] and nanographene, a promising near-infrared emitting probe for intravital imaging.[7] Metallic nanoparticles, including Au and Ag, have also been engineered as probes for high-resolution optical imaging and

Received: July 23, 2013
Accepted: August 29, 2013
Published: August 29, 2013

generate unique and tunable signals due to specific surface plasmon resonance (SPR).[8−11] In particular, silver nanoparticles (AgNPs) can be imaged within labeled cells by using dark-field microscopy (DFM)[12−14] or SERS microscopy because of the generation of specific SPR signals.[15,16] DFM is a remarkably powerful yet simple technique that uses a low energy of the NIR source to record signals and molecular properties from individual NPs in a cell.[17−19] SERS imaging microscopy also allows the user to image a single NP while the intrinsic molecular specificity of the SERS signal is used for the detection and sensing of specific DNA and proteins in cells, or to dynamically monitor enzyme activity and metabolites, including glucose.[20−23]

An ideal probe for multiscale imaging of a biological sample is one that combines several of the contrast-enhancing advantages based on the imaging modalities mentioned above. This new class of probe could generate new structural and chemical information over multiple scales of space and time. A microbubble (MB) probe, stabilized by an outer shell composed of proteins, lipids, surfactants, or biocompatible polymers,[24,25] would be an excellent multifunctional platform for applications in ultrasound medical imaging, multimodal imaging, and drug delivery.[26−28] The aim of this study is to develop a new class of multifunctional microbubble probes for multiscale imaging of biological samples. The structural design of these probes involves harboring a large number of AgNPs within a polymer shell. In this study, we mainly focus on the preparation and characterization of AgNP-embedded MB probes and provide a proof-of-principle application to demonstrate their potential as probes for ultrasound imaging, ultrasound-mediated delivery of AgNPs to cells, and high-resolution DFM, SERS-based imaging, and chemical sensing of AgNPs within living cells.

2. EXPERIMENTAL SECTION

Materials. Polyvinyl alcohol (PVA) (MW = 31000 and 110000) was purchased from Sigma-Aldrich; poly(D,L)-lactide (PLA) (MW = 15000) was purchased from Shandong Daigang. Nile Blue A (NBA) was purchased from Alfa Caesar. Span 80, Tween 80, N_2, and all other chemicals were analytical reagent grade and used as received.

Electrochemical Synthesis of AgNPs. PVA-coated AgNPs were synthesized by using the electrochemical method. Two grams of PVA (MW = 110000) was dissolved in distilled water (200 mL) and magnetically stirred in a beaker at 75 °C. Two silver electrodes (Changshu Changhong Precious Metal Co., Ltd.) with a spacing of 2 cm were positioned within the beaker, and a dc voltage of 25 V was applied for 3 min. The aqueous colloidal suspension of silver nanoparticles that formed after this operation was purified and used without any further treatment.

Fabrication and Characterization of AgNP-Embedded MBs. AgNP-embedded MBs were fabricated by using a method similar to that detailed by our laboratory.[29] Briefly, PLA (0.50 g) was dissolved in 10 mL of methylene chloride at 25 °C. The first emulsion was generated by adding Milli-Q water (1.00 mL) and Span 80 (0.05 mL) to the organic solution that was being continuously stirred at high speed. This emulsion was poured into a 1% solution of PVA [50 mL, MW = 31000 (w/v)] with a solution of PVA-coated AgNPs [1 mL, MW = 110000 (w/v)] and mechanically stirred for 2 h, after which it formed a stable emulsion. Control samples lacking AgNPs were prepared by using the same procedure. Free PVA and AgNPs were removed from the emulsion, and the resultant microcapsules were suspended in a phosphate-buffered solution (PBS, pH 7.4) followed by centrifugation and washed three times in PBS. The purified AgNP-embedded MB solution was stored in mannitol, which serves as a preservative, and was subsequently lyophilized (FreeZone freeze-dryer, LABCONCO). After the drying process had been completed, vials were flushed with N_2 and tightly sealed.

The size distribution of purified MBs was analyzed by using a 90Plus Particle Size Analyzer (Brookhaven Instrument Corp.). Freshly prepared MBs were first diluted to the required concentration and measured by using a hemocytometer. The weight content of AgNPs embedded within the shell of the MBs was determined by using an atomic absorption spectrometer (model 180-80, Hitachi). The morphology and structure of the MBs were studied with a scanning electron microscope (SEM). The structure of the polymer shell in MBs is imaged as follows. Lyophilized MB samples were sectioned by using a resin embedding method. In particular, samples were fixed in 1% OsO_4 for 1 h, dehydrated in acetone, and subsequently embedded in a liquid epoxy resin. After hardening, the resin blocks were sectioned (at 50 nm units) and stained with uranyl acetate and lead citrate before being imaged. The presence of AgNPs in the MB shell was confirmed by characterizing noble metals within MBs by means of an energy dispersive X-ray analysis (EDXA, FEI XL30).

***In Vitro* Acoustic Imaging Experiments.** *In vitro* acoustic imaging experiments were performed by using a homemade agar power phantom. Samples were tested and imaged by using a digital B-mode diagnostic ultrasonic instrument (Belson 3000A, Belson Imaging Technology Co., Ltd., Wu Xi, China) with a 3.5 MHz R60 convex array probe. A dilute suspension of MBs was injected into the pipeline of the phantom imaged by ultrasound every 10 s. A purposefully designed MATLAB computer program that analyzed values from a mean gray scale was used to quantitatively measure the brightness of samples in the image. The mean gray scale was calculated as the average of the gray scale levels of all pixels within a region of interest (ROI). Mean gray scale values within a ROI were calculated automatically with this MATLAB program. Three scanned segments (ROI) were processed for each sample, and the average mean gray scale was used for that particular sample. Distilled and degassed water was used as a control sample for these studies. The studies included authentic AgNP-MBs and MBs without AgNPs. The MB solution was adjusted to a density of $1-6 \times 10^6$ MBs/mL. All measurements were recorded under the same conditions of temperature, ultrasound exposure, and solvent composition.

UV−Vis Absorption Spectra, DFM Studies, and SERS Studies. UV−vis absorption spectra were recorded using a UV-3600 spectrophotometer (Shimadzu).

The identification of AgNPs within a MB was established by using DFM imaging using an inverted microscope (Carl Zeiss). A high-numerical aperture objective (NA 0.8, 4×) was used with a white light source and a digital camera to image scattered light from AgNPs in reflection mode. The MB solutions or cell solutions were placed onto a clean glass slide for these imaging studies.

SERS studies were conducted using MBs that either contained or lacked AgNPs. The MB sample (~0.2 mL) was placed onto a glass slide and covered with a coverslip. To evaluate the SERS characteristics of the samples, the NBA probe molecules were mixed with the samples before being deposited on the glass. The SERS peak for samples containing NBA was expected to occur at 592 cm^{-1}. SERS spectra resulting from an exposure of the AgNPs to a 785 nm He−Ne laser were acquired by using a Micro-Raman Spectroscopy System (Renishaw Invia Reflex System) that continuously recorded background-corrected spectra. Spectra were fit to mixed Gaussian and Lorentzian modes using the Renishaw Wire software. The extracted data were further analyzed using Origin version 7.5.

Interaction between AgNP-Embedded MBs and Tumor Cells under Ultrasound Exposure. SMMC-7721 cells (a human liver carcinoma cell line) were purchased from the Cell Bank of Type Culture Collection of the Chinese Academy of Sciences (Shanghai, China). The cells were cultured as monolayers in RPMI 1640 medium and 10% fetal bovine serum (FBS) and maintained in a humidified 5% CO_2 atmosphere at 37 °C. Exponentially growing cells were harvested and resuspended in fresh RPMI 1640 medium with 10% FBS. The number of cells was adjusted to $1-6 \times 10^6$ cells/mL. The ratio of MBs to cells was ~10:1. For each trial, 1 mL of the cell suspension with 0.1 mL of the MB solution were placed into a plastic tube 15 mm in

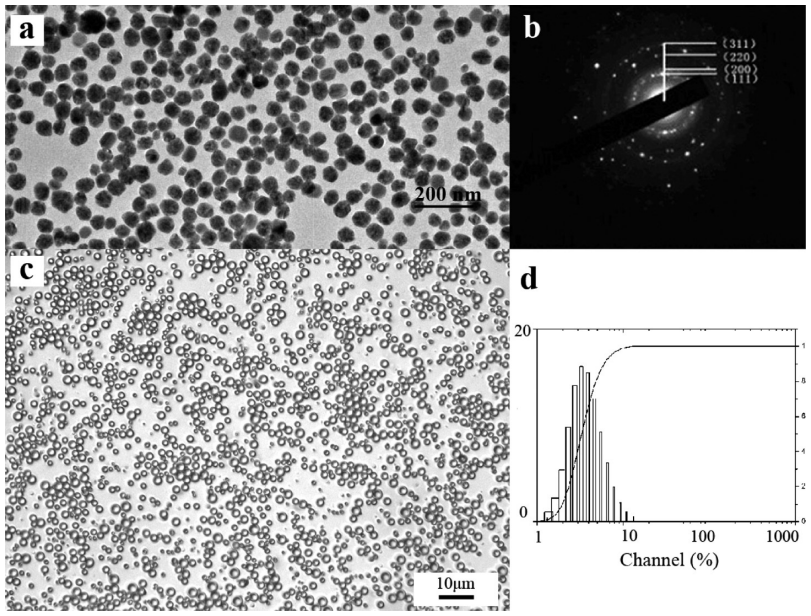

Figure 1. (a) TEM image of AgNPs synthesized at 75 °C stabilized by PVA (MW = 110000). The statistical analysis of >1000 particles reveals a mean diameter of 50.1 ± 4.4 nm. (b) SAED pattern of AgNPs. The electron diffraction rings are indexed to the (111), (200), (220), and (311) crystalline planes of silver. (c) Microscopy image of AgNP-embedded MBs under an optical bright field showing a spherical morphology. (d) The size distribution of the MBs was within the range of 2−5 μm (mean diameter of 4.15 μm).

diameter and 75 mm in length (Kimble, Owens-Illinois, Toledo, OH) with a sound transparent polymer membrane bottom. The ultrasound exposure system has been described previously.[30] Briefly, a 1 MHz unfocused 30 mm diameter single-element transducer (Yu-Chao Electronics Co., Ltd., Wu Xi, China) was positioned in a water tank. The transducer was connected to an arbitrary waveform generator (model 33250A, Agilent) and a 50 dB broadband RF power amplifier (model 2100L, ENI, Rochester, NY). Cells were exposed to sine wave of ultrasound tone bursts with 20 cycles per tone burst at a pulse repetition frequency (PRF) of 10 kHz. The ultrasound spatial and temporal averaged intensity used in the experiments was 0.5 W/cm^2, a level that was verified with a calibrated hydrophone (TNU0001A, NTR, Seattle, WA). The sample was exposed to ultrasound for total of 40 s.

3. RESULTS AND DISCUSSION

General Characterization of PVA-Coated AgNPs and AgNP-Embedded MBs. The TEM image of these AgNPs is shown in Figure 1a with the selected area electron diffraction (SAED) patterns of the same AgNPs shown in Figure 1b. The mean diameter of AgNPs was 50 nm measured by TEM images. The SAED patterns are indexed to the (111), (200), (220), and (311) crystalline planes of silver, which suggests the PVA-stabilized AgNPs have defined structure and morphology.

Analysis of a large population of AgNP-embedded MBs shown in the bright-field image of Figure 1c indicates that the MBs are spherical in shape. A statistical analysis of the size distribution of MBs is shown in Figure 1d, which reveals a mean diameter of 4.15 μm with a range from 2 to 5 μm. The weight concentration of Ag encapsulated in the shell was calculated as 82.4 μg/mL of MB solution based on atomic absorption spectrometer measurements. Because the number concentration of MBs in the solution is 2−6 × 10^6 MBs/mL, the weight concentration of AgNPs within one MB is 41.2 × 10^{-6} to 13.7 × 10^{-6} μg.

Nanoscale Structural and Chemical Characterization of AgNP-Embedded MBs. The morphology of the shape and shell structure of the MBs with or without embedded AgNPs was examined with a SEM. The morphology of MBs without AgNPs is generally spherical with a relatively smooth surface (Figure 2a,c). On the other hand, the surface of MBs embedded with AgNPs is coarse and pitted with craterlike features (Figure 2b). Next we recorded magnified SEM images of sectioned MB samples to better characterize the ultrastructure of these MBs. These studies reveal a double-shell structure within MBs (Figure 2c,d). Moreover, images of these sectioned MBs suggest that AgNPs are contained within the outermost layer of the MB shell (arrows in Figure 2d), whereas control MBs do not show evidence of any nanoparticles. Imaging studies using energy dispersive X-ray analysis (EDXA) further confirmed conclusions drawn from the bright-field and SEM studies detailed above. In particular, the spectral data indicate that the shell of AgNP-embedded MBs contains carbon, oxygen, and silver (Figure 2e) and the peak from silicon is most likely arising from the substrate.

***In Vitro* Ultrasound Imaging.** B-Mode ultrasound images of control and AgNP-embedded MBs in solution are shown in Figure 3. These studies demonstrate that AgNP-embedded MBs have a greater mean gray scale value (103.74 ± 3.19) than MBs without AgNPs (60.56 ± 4.05). The mean gray scale value of deionized and degassed water of 14.37 ± 1.97 reflects a uniform propagation of an ultrasonic wave. Other studies have shown that the presence of NPs on the surface of a MB can change its viscoelastic properties and strengthen the nonlinear echogenic character of the MBs when they are exposed to ultrasound,[31,32] with higher-contrast enhancements arising from the larger ultrasound echo contributions from AgNPs in the MB shell. Consequently, we can conclude that AgNP-embedded MBs can also exhibit improved contrast enhancement for ultrasound-based imaging of subjects.

Optical Imaging of AgNPs within MBs. The optical imaging enhancement of AgNP-embedded MBs was investigated by using DFM and SERS microscopy. A dark-field image of a typical preparation of MBs harboring AgNPs is shown in Figure 4a. Although the average diameter of prepared

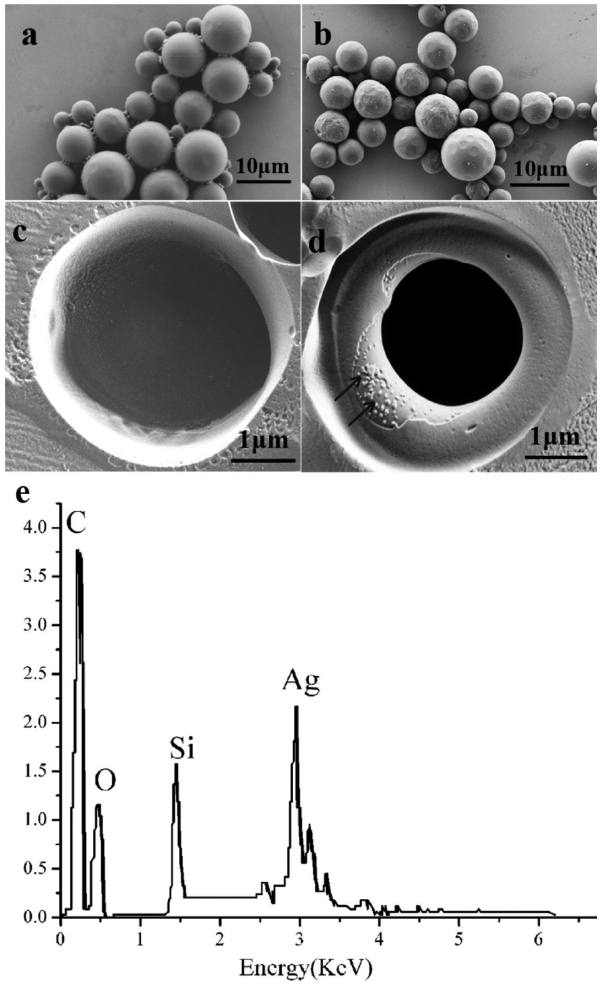

Figure 2. SEM images of MBs: (a) MBs without AgNPs and (b) AgNP-embedded MBs. (c and d) Enlarged magnifications of sectioned MB samples that clearly reveal NPs in the shell (arrows). (e) The EDXA spectrum of AgNP-embedded MBs clearly reveals that the AgNP-embedded MBs consist of Ag along with C, O, and Si.

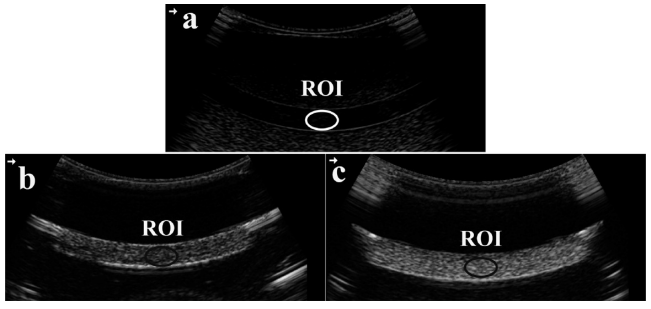

Figure 3. B-Mode ultrasound images in the different samples *in vitro*: (a) deionized and degassed water, (b) MBs without AgNPs, and (c) AgNP-embedded MBs. The mean gray scale was calculated as the average of the gray scale levels of all pixels within a region of interest (ROI). The contrast enhancement can be quantitatively measured according to the brightness of samples in the ROI of the image.

colloidal AgNP is ~50 nm (Figure 1a), once integrated within the shell of a MB, these particles likely aggregate or cluster to form an array of larger structures (Figure 2d) that exhibit a range of red-shifted plasmon resonances. The aggregated structures of AgNPs in the MB shell generate a multitude of colors in the polymer shell of the MB when viewed via DFM (Figure 4a). The optical DFM results demonstrate two principles. First, AgNPs in the MB shell can be in the presence of different sizes and structures. DFM imaging can be used to analyze the organization of AgNPs in the polymer shell of MBs. Second, AgNP-embedded MBs can also serve as useful probes for DFM-based imaging of MBs, while their release following exposure to ultrasound may be used to deliver the probe to living cells.

The UV−vis spectra of pure AgNPs in solution and MBs with and without AgNPs are shown in Figure 4b. The results show that the pure AgNPs solution has a maximal absorption at 433 nm with half-maximal width of 45 nm. No absorption peaks are evident in the spectrum of the control sample [MBs without AgNPs (red line)]. The absorption spectrum of AgNP-embedded MBs (black line) is very similar to that measured for the pure AgNPs solution (green line). Compared to AgNPs alone, AgNP-embedded MB solution has a lower extinction intensity and a broader half-maximal width of 68 nm. The value of the half-maximal width reflects the heterogeneity of ground states, and because this value is higher for AgNP-embedded MBs, this result supports the DFM study (Figure 4a) that found the aggregation of AgNPs within the polymer shell of MBs.

SERS spectroscopy is used to provide details about specific interactions between the surface of the AgNP and molecules in the MB. The high specificity and strong intensity of the SERS spectrum of NBA at 592 cm^{-1} are used as an intensity reference for this study. The SEM image of MBs on a silicon substrate is shown in Figure 5a. Representative SERS spectra obtained from AgNPs and MBs with or without AgNPs are shown in Figure 5b. The Raman spectrum of MBs without AgNPs (red trace) lacks structure and had no signal at the 592 cm^{-1} peak. On the other hand, the optoelectronic property of MBs harboring AgNPs exhibits a rich SERS spectrum with a characteristic Raman peak at 592 cm^{-1}. Although the peak intensity at 592 cm^{-1} for this sample is lower (7898) compared to that measured for pure AgNPs (17525, green trace), this signal from the Raman peaks in the spectrum can be used for the rapid and sensitive detection of AgNP-embedded MBs. The binding of specific molecules onto, or near, the surface of the SERS substrate generates a new SERS peak whose intensity correlates with the number of absorbed molecules.[33] This feature, however, means that SERS substrates are also sensitive to the binding of nontarget molecules. The AgNPs within the polymer shell of the MB provide some protection against the effects of nonspecific binding when compared to free AgNPs. Moreover, the aggregation of AgNPs within the MB shell (Figures 2d and 4a) that results in a red shift absorption may enhance the SERS detection associated with the binding of a target molecule.[34] Finally, we note that the polymer shell is capable of protecting the embedded AgNPs from oxidation by molecular oxygen, which should increase the stability of AgNPs for SERS detection.

AgNP-Embedded MBs as Optical Probes within Living Cells. As discussed earlier, the binding of specific molecules to the surface of a nanoparticle will generate new SERS signals that can be analyzed to identify the bound molecule. This feature has been used to study SERS-based intracellular chemical sensors of proteins and metabolites within living cells.[35] In this section, we describe how MBs embedded with AgNP serve as multifunctional probes for ultrasound-mediated delivery of AgNPs to living cells and SERS-based analysis of intracellular molecules. First, we exposed a suspension of MBs

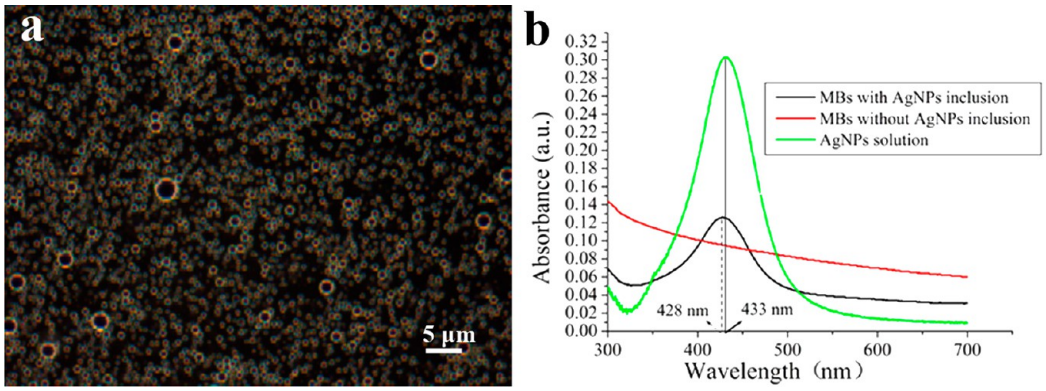

Figure 4. Dark-field scattering images and UV−vis spectra of MBs with or without AgNPs. (a) Colorful rainbow ring image of a typical AgNP-embedded MB sample under DFM, which reflects the presence of aggregated forms of AgNPs in the shell of AgNP-embedded MBs. (b) UV−vis spectra of pure AgNPs in solution (green) and MBs with (black) and without (red) AgNPs. The absorption spectrum of AgNP-embedded MBs is very similar to that measured for the pure AgNP solution except that the AgNP-embedded MB solution has a lower extinction intensity and a broader half-maximal width.

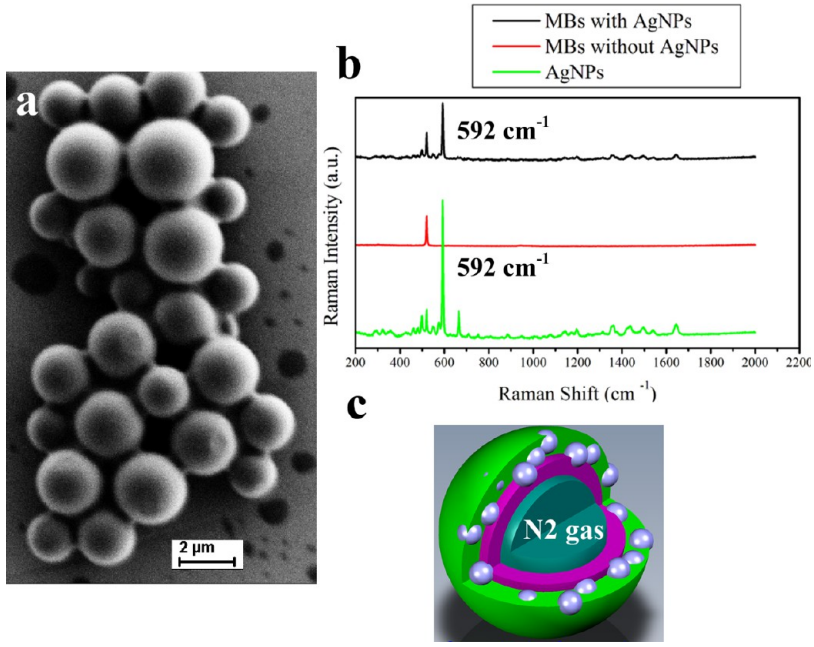

Figure 5. (a) SEM image of a AgNP-embedded MB sample on a silicon substrate. (b) Background-corrected Raman spectrum of pure AgNPs and MBs with or without AgNPs obtained by using 785 nm laser excitation. MBs harboring AgNPs exhibit a rich SERS spectrum with a characteristic Raman peak at 592 cm^{-1}. (c) Schematic diagram of AgNP-embedded MBs, which shows the shell encapsulation and the distribution of the AgNPs in the shell.

embedded with AgNPs to a brief pulse of ultrasound at a power level of 0.5 W/cm^2 in the vicinity of surface-attached SMMC-7721 liver tumor cells. The collapse of the MB liberates the AgNPs from the MB shell and results in their delivery to individual cells. Next, we analyzed the distribution and surface properties of intracellular AgNPs by using DFM, which revealed their distribution, and by SERS to identify unique peaks associated with the binding of specific molecules to the surface of the AgNP. A population of labeled cells is shown in Figure 6a, which was generated by overlapping bright-field and dark-field images of the same samples. The false color overlap image highlights both free and aggregated AgNPs within labeled cells.

SRES spectra recorded from these intracellular AgNPs are analyzed to indentify molecules that bind to the AgNP surfaces. A typical SERS spectrum recorded from AgNPs within a living cell is shown in Figure 6b. Analysis of this SERS spectrum reveals the presence of new peaks at 236, 464, 509, 655, 781, 825, 933, 1002, 1098, 1117, 1245, 1339, 1396, 1453, and 1575 cm^{-1}. These peaks are found to correspond to the binding of biomolecules one might expect to find within a living cell: for example, the 1245 cm^{-1} peak indicates the presence of bound proteins, while the 1002 and 825 cm^{-1} peaks represent Phe and Tyr, respectively.[36] Moreover, the 1098 and 1580 cm^{-1} peaks are indicative bound nucleic acids. The significance of these peaks is shown by the fact that they are not present in the SERS spectra of a control AgNP (added to the extracellular space). Moreover, a second control spectrum that is recorded from MBs without AgNPs does not show any specific SERS enhancements in the Raman spectrum. We conclude, therefore, that intracellular AgNP probes in conjunction with SERS spectroscopy and DFM can rapidly provide detailed informa-

dx.doi.org/10.1021/am4029747 | ACS Appl. Mater. Interfaces 2013, 5, 9217−9223

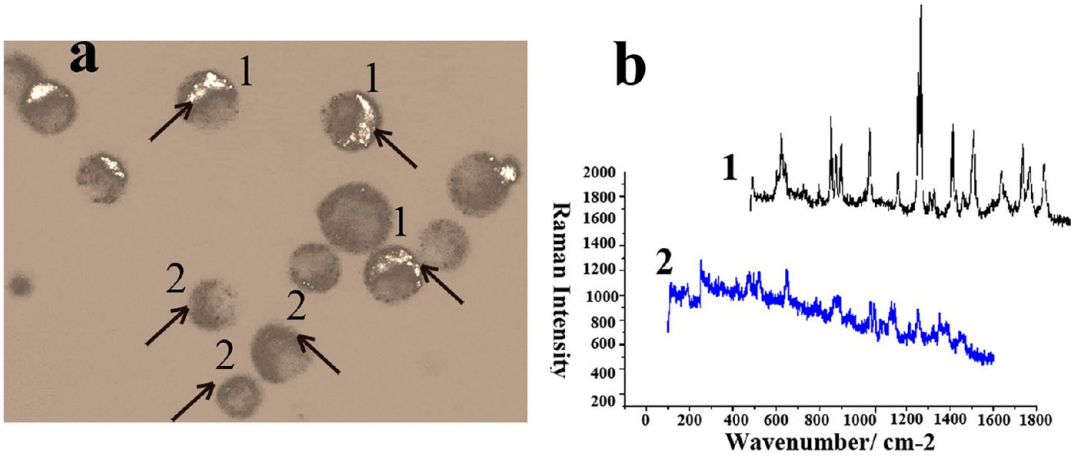

Figure 6. Dark-field scattering images and SERS spectra of SMMC-7721 cells. (a) Overlap image of SMMC-7721 cells under white light microscopy and dark-field microscopy. (b) SERS detection of SMMC-7721 cells with (1) and without (2) AgNPs.

tion about the distribution of individual AgNPs within living cells with a high spatiotemporal resolution and allow the user to identify molecules that bind to the surface of intracellular molecules of these AgNPs.

4. CONCLUSIONS

Multifunctional probes that provide high contrast over multiple scales of space and time are key for multiscale imaging and diagnosis of a living system. In this report, we describe a new class of multifunctional, contrast-enhancing probe that combines features that are suitable for both ultrasound and optical imaging modalities for multiscale biomedical imaging and probe or drug delivery. The structural design of these multifunctional probes is unique and involves encapsulating a nitrogen gas core within a biocompatible polymer shell that harbors a large number of individual and aggregated AgNPs. The ultrasound studies of MBs are used to show that the presence of AgNPs significantly improves contrast enhancement. Exposing a suspension of MBs to ultrasound is shown to release AgNPs into the medium, where they are taken up by surface-attached cells. These intracellular AgNPs are imaged using DFM, while SERS is used to identify specific cytoplasmic biomolecules that bind to the AgNP surface. Multimodal imaging techniques are employed to demonstrate the potential of our new class of multifunctional MB for multiscale (micrometer to nanometer) imaging and chemical analysis of specific biomolecules within living cells. Future studies will involve linking MBs with specific antibodies that are directed against surface proteins on tumor cells in an effort to target the MB to the tumor.

AUTHOR INFORMATION

Corresponding Authors

*School of Biological Science and Medical Engineering, Southeast University, Nanjing 210096, P. R. China. Fax: +86-25-83272460. Telephone: +86-25-83272476. E-mail: yangfang2080@seu.edu.cn.

*School of Biological Science and Medical Engineering, Southeast University, Nanjing 210096, P. R. China. Fax: +86-25-83272460. Telephone: +86-25-83272460. E-mail: guning@seu.edu.cn.

Notes

The authors declare no competing financial interest.

ACKNOWLEDGMENTS

This work was supported by the National Key Basic Research Program of China (2011CB933503 and 2013CB733804), the National Natural Science Foundation of China (31000453 and 31370019), the Foundation for the Author of National Excellent Doctoral Dissertation of P. R. China (201259), the Specialized Research Fund for the Doctoral Program of Higher Education of China (20100092120038), and the Fundamental Research Funds for Central Universities (2013CB733804). We would like to thank Prof. Yuling Yan from the Department of Bioengineering at Santa Clara University for helpful discussions and suggestions.

ABBREVIATIONS

MBs, microbubbles
AgNPs, silver nanoparticles
CT, computed tomography
US, ultrasound
MRI, magnetic resonance imaging
SPECT, single-photon emission-computed tomography
PET, positron emission tomography
SPR, surface plasmon resonance
SERS, surface-enhanced Raman scattering
NIR, near-infrared
DFM, dark-field microscopy
NBA, Nile Blue A

REFERENCES

(1) Sutton, J. T.; Haworth, K. J.; Pyne-Geithman, G.; Holland, D. C. K. *Expert Opin. Drug Delivery* **2013**, *10*, 573−592.
(2) Wilson, S. R.; Burns, P. N. *Radiology* **2010**, *257*, 24−39.
(3) Louie, A. *Chem. Rev.* **2010**, *110*, 3146−3195.
(4) Moon, H. K.; Lee, S. H.; Choi, H. C. *ACS Nano* **2009**, *3*, 3707−3713.
(5) Backes, C.; Englert, J. M.; Bernhard, N.; Hauke, F.; Hirsch, A. *Small* **2010**, *6*, 1968−1973.
(6) Pribiag, V. S.; Nadj-Perge, S.; Frolov, S. M.; van den Berg, J. W. G.; van Weperen, I.; Plissard, S. R.; Bakkers, E. P. A. M.; Kouwenhoven, L. P. *Nat. Nanotechnol.* **2013**, *8*, 170−174.
(7) Yang, K.; Feng, L.; Shi, X.; Liu, Z. *Chem. Soc. Rev.* **2013**, *42*, 530−547.
(8) Baudrion, A. L.; Perron, A.; Veltri, A.; Bouhelier, A.; Adam, P. M.; Bachelot, R. *Nano Lett.* **2013**, *13*, 283−286.
(9) Henry, A. I.; Bingham, J. M.; Ringe, E.; Marks, L. D.; Schatz, G. C.; Van Duyne, R. P. *J. Phys. Chem. C* **2011**, *115*, 9291−9305.

(10) Si, P.; Huang, Y.; Wang, T.; Ma, J. *RSC Adv.* **2013**, *3*, 3487−3502.
(11) Song, J.; Kang, H.; Lee, C.; Hwang, S. H.; Jang, J. *ACS Appl. Mater. Interfaces* **2012**, *4*, 460−465.
(12) Sunaguchi, N.; Yuasa, T.; Huo, Q.; Ichihara, S.; Ando, M. *Appl. Phys. Lett.* **2011**, *99*, 103704−104704-3.
(13) Liu, Q.; Wei, L.; Wang, J.; Peng, F.; Luo, D.; Cui, R.; Niu, Y.; Qin, X.; Liu, Y.; Sun, H.; Yang, J.; Li, Y. *Nanoscale* **2012**, *4*, 7084−7089.
(14) Yang, Y.; Li, Z.; Yamaguchi, K.; Tanemura, M.; Huang, Z.; Jiang, D.; Chen, Y.; Zhou, F.; Nogami, M. *Nanoscale* **2012**, *4*, 2663−2669.
(15) Qian, X. M.; Nie, S. M. *Chem. Soc. Rev.* **2008**, *37*, 912−920.
(16) Ye, S.; Yang, Y.; Xiao, J.; Zhang, S. *Chem. Commun.* **2012**, *48*, 8535−8537.
(17) Guo, L.; Ferhan, A. R.; Lee, K.; Kim, D. H. *Anal. Chem.* **2011**, *83*, 2605−2612.
(18) Novo, C.; Funston, A. M.; Pastoriza-Santos, I.; Liz-Marzan, L. M.; Mulvaney, P. *Angew. Chem., Int. Ed.* **2007**, *46*, 3517−3520.
(19) Krishnaswamy, V.; Laughney, A. M.; Paulsen, K. D.; Pogue, B. W. *Opt. Lett.* **2011**, *36*, 1911−1913.
(20) Kim, K.; Shin, K. S. *Anal. Sci.* **2011**, *27*, 775−783.
(21) Singh, R.; Nalwa, S. H. *J. Biomed. Nanotechnol.* **2011**, *7*, 489−503.
(22) Li, J. F.; Huang, Y. F.; Ding, Y.; Yang, Z. L.; Li, S. B.; Zhou, X. S.; Fan, F. R.; Zhang, W. *Nature* **2010**, *464*, 392−395.
(23) Zhang, Y.; Hong, H.; Myklejord, D. V.; Cai, W. *Small* **2011**, *7*, 3261−3269.
(24) Geis, N. A.; Katus, H. A.; Bekeredjian, R. *Curr. Pharm. Des.* **2012**, *18*, 2166−2183.
(25) Unnikrishnan, S.; Klibanov, A. L. *Am. J. Roentgenol.* **2012**, *199*, 292−299.
(26) Suzuki, R.; Oda, Y.; Utoguchi, N.; Maruyama, K. *J. Controlled Release* **2011**, *149*, 36−41.
(27) Deelmana, L. E.; Declèvesb, A. E.; Rychakc, J. J.; Sharma, K. *Adv. Drug Delivery Rev.* **2010**, *62*, 1369−1377.
(28) Cavalieri, F.; Micheli, L.; Kaliappan, S.; Teo, B. M.; Zhou, M.; Palleschi, G.; Ashokkumar, M. *ACS Appl. Mater. Interfaces* **2013**, *5*, 464−471.
(29) Yang, F.; Li, Y.; Chen, Z.; Zhang, Y.; Wu, J.; Gu, N. *Biomaterials* **2009**, *30*, 3882−3890.
(30) Yang, F.; Zhang, M.; He, W.; Chen, P.; Cai, X.; Yang, L.; Gu, N.; Wu, J. *Small* **2011**, *7*, 902−910.
(31) Sassaroli, E.; Li, K. C. P.; O'Neill, B. E. *J. Acoust. Soc. Am.* **2009**, *126*, 2802−2813.
(32) Stride, E.; Pancholi, K.; Edirisinghe, M. J.; Samarasinghe, S. *J. R. Soc., Interface* **2008**, *5*, 807−811.
(33) Schlücker, S. *ChemPhysChem* **2009**, *10*, 1344−1354.
(34) Su, X.; Zhang, J.; Sun, L.; Koo, T. W.; Chan, S.; Sundararajan, N.; Yamakawa, M.; Berlin, A. A. *Nano Lett.* **2005**, *5*, 49−54.
(35) Lee, S. E.; Sasaki, D. Y.; Park, Y.; Xu, R.; Brennan, J. S.; Bissell, M. J.; Lee, L. P. *ACS Nano* **2012**, *6*, 7770−7780.
(36) Ross, B. M.; Waldeisen, J. R.; Wang, T.; Lee, L. P. *Appl. Phys. Lett.* **2009**, *95*, 193112.